AIP | Journal of Applied Physics

Direct observation of enhanced emission sites in nitrogen implanted hybrid structured ultrananocrystalline diamond films

Kalpataru Panda, Huang-Chin Chen, B. Sundaravel, B. K. Panigrahi, and I.-Nan Lin

Citation: Journal of Applied Physics **113**, 054311 (2013); doi: 10.1063/1.4790481
View online: http://dx.doi.org/10.1063/1.4790481
View Table of Contents: http://scitation.aip.org/content/aip/journal/jap/113/5?ver=pdfcov
Published by the AIP Publishing

Direct observation of enhanced emission sites in nitrogen implanted hybrid structured ultrananocrystalline diamond films

Kalpataru Panda,[1,a)] Huang-Chin Chen,[2] B. Sundaravel,[1] B. K. Panigrahi,[1,b)] and I.-Nan Lin[2]
[1]*Materials Physics Division, Indira Gandhi Centre for Atomic Research, Kalpakkam 603 102, India*
[2]*Department of Physics, Tamkang University, New-Taipei 251, Taiwan*

(Received 30 November 2012; accepted 22 January 2013; published online 6 February 2013)

A hybrid-structured ultrananocrystalline diamond (h-UNCD) film, synthesized on Si-substrates by a two-step microwave plasma enhanced chemical vapour deposition (MPECVD) process, contains duplex structure with large diamond aggregates evenly dispersed in a matrix of ultra-small grains (~5 nm). The two-step plasma synthesized h-UNCD films exhibit superior electron field emission (EFE) properties than the one-step MPECVD deposited UNCD films. Nitrogen-ion implantation/post-annealing processes further improve the EFE properties of these films. Current imaging tunnelling spectroscopy in scanning tunnelling spectroscopy mode directly shows increased density of emission sites in N implanted/post-annealed h-UNCD films than as-prepared one. X-ray photoelectron spectroscopy measurements show increased sp^2 phase content and C–N bonding fraction in N ion implanted/post-annealed films. Transmission electron microscopic analysis reveals that the N implantation/post-annealing processes induce the formation of defects in the diamond grains, which decreases the band gap and increases the density of states within the band gap of diamond. Moreover, the formation of nanographitic phase surrounding the small diamond grains enhanced the conductivity at the diamond grain boundaries. Both of the phenomena enhance the EFE properties. © *2013 American Institute of Physics*. [http://dx.doi.org/10.1063/1.4790481]

I. INTRODUCTION

Ultra-nanocrystalline diamond (UNCD) film is a special form of diamond that has recently caught great attention from researchers because of its better electron field emission (EFE) properties.[1] The UNCD film has ultra-small diamond grain (2–5 nm) and very smooth surface characteristics.[1] The grains are diamond, having a sp^3 character and the grain boundaries have a mixture of sp^2, sp^3, and amorphous carbon with sp^2 character being predominant.[2] The decrease in diamond grain size increases the grain boundary (GB) volume fraction that contains the non-diamond carbon, resulting in significant improvement in electrical properties for these films. The non-diamond phase content plays a crucial role for the EFE properties of diamond films.[1] In an effort to increase the non-diamond phase content and thus to improve the EFE properties of diamond films, we have carried out a modified nucleation and growth process, where a UNCD film grown in $CH_4/Ar = 4/196$ sccm plasma is used as the nucleation layer for the growth of diamond film in the same microwave plasma enhanced chemical vapour deposition (MPECVD) chamber in $CH_4/Ar/H_2 = 1/50/49$ sccm plasma.[3–5] Such a two-step MPECVD process resulted in hybrid-UNCD (h-UNCD) diamond film with very unique granular structure, which neither contains micron sized nor ultrananno-sized diamond grains. These films contained large diamond aggregates dispersed among the ultra-small diamond (~5 nm) matrix. Such kind of hybrid granular structured UNCD films exhibits better EFE properties than the conventional micro-, nano-, or ultrananno-crystalline diamond films.[3–5] However, the resulted EFE properties are still not satisfactory, as compared with those of nano-carbon materials,[6–8] indicating that there is still room for improvement. Ion implantation was extensively used in the past to dope bulk diamond to enhance their electrical properties.[9–12] N-ion implantation to hybrid-UNCD films seems to be a probable approach for further enhancing the EFE properties of these thin diamond materials.

In this context, we report a detailed study on the effect of N ion implantation and subsequent post-annealing (N-ion implantation/post-annealing) processes in modifying the microstructure and EFE properties of h-UNCD films, which were prepared by a two-step MPECVD process. Importantly, current imaging tunnelling spectroscopy (CITS) in scanning tunnelling spectroscopy (STS) mode is used to directly detect the increased emission site densities in N implanted/post-annealed films than the as-prepared ones in nanometre scale. High resolution transmission electron microscopy (HRTEM) is used to investigate the microstructural evolution of the film surface after the N implantation/post-annealing processes. Further, the possible mechanism for enhancement in EFE properties of these hybrid films is discussed on the basis of the experimental observations.

II. EXPERIMENTAL

Diamond films were grown on n-type mirror polished Si (100) substrates. The UNCD films were used as a nucleation layer to promote the growth of diamond films on it. The UNCD nucleation layer was grown on Si-substrates by MPECVD process, in Ar-rich plasma ($CH_4/Ar/H_2 = 4/196/0$ sccm) conditions (1200 W, 133 mbar, 60 min) to a thickness of 1 μm. The growth process was carried out at low temperatures of 480 °C without any intentional heating of the substrates.

[a)]Electronic mail: phy.kalpa@gmail.com.
[b)]Electronic mail: bkp@igcar.gov.in.

Growth of the secondary diamond films on UNCD nucleation layer was carried out in the same MPECVD processor using H_2-riched plasma ($CH_4/Ar/H_2 = 1/49/50$ sccm, 73 mbar) with 1600 W microwave power for 60 min. The total thickness of the film after the secondary diamond film deposition is 1.7 μm. Such a process modified the granular structure of UNCD layer, rather than forming a large diamond grain layer on top of UNCD films.[3–5] Thus, obtained composite films were designated as hybrid-UNCD films. A 150 kV ion implanter was used to implant 75 keV nitrogen ions with an ion fluence of 5×10^{15} ions/cm^2 on h-UNCD films at room temperature and a pressure below 2×10^{-7} mbar. This fluence was so chosen as a critical dose of over 1×10^{15} ions/cm^2 is required to improve the EFE properties of UNCD films.[11] After implantation, the films were annealed at 800 °C in N_2 atmosphere for 30 min.

Field emission experiments were carried out in a home-made tuneable parallel plate capacitor setup. The separation between the anode (Mo) tip and the sample was measured using a digital micrometer and an optical microscope. The EFE properties were analyzed by Fowler–Nordheim (F–N) model.[13] The turn-on field is designated as the interception of the high and low-field segments of the F–N plots. The surface morphology of as-prepared, N ion implanted, and post-annealed hybrid-UNCD films was investigated by field emission scanning electron microscope (FESEM, CARL ZEISS, SUPRA 55). The Raman spectra were recorded by using 514.5 nm line of an Ar-ion laser in Renishaw micro-Raman spectrometer (Model-INVIA). The chemical bonding structures were investigated by X-ray photoelectron spectroscopy (XPS, SPECS, Germany). This spectrometer uses monochromatic Al Kα radiation at 1486.74 eV as a probe. The detailed microstructures of h-UNCD films are examined by transmission electron microscope (TEM, Joel 2100).

Scanning tunnelling microscopy (STM) measurements were carried out in a UHV-STM apparatus (150 Aarhus, SPECS GmbH, Germany) at 10^{-10} mbar pressure. The STS spectra were obtained during scanning and the data presented here are reproducible over subsequent scans. CITS in STS mode was carried out to correlate the STM images with its surface local density of states (DOS) distributions.[13] CITS involves acquiring, a current versus voltage (I-V) curve, in each point of the scanned surface while the feedback loop is off.

III. RESULTS

A. Material characteristics

The effect of N ion implantation and post-annealing processes in modifying the EFE properties of h-UNCD films is shown in Fig. 1 with the inset indicating the corresponding F–N plot, the variation of ln(J/E^2) versus 1/E, of the corresponding field emission (J-E) curves. The turn-on field (E_0) designated here is the lowest value of the F–N plot, corresponding to the intersection of the low and high electric field segments. This figure shows that the turn-on field (E_0) decreases from 10.3 V/μm for as-prepared h-UNCD films (curve I) to 7.4 V/μm for N-ion implanted/post-annealed films (curve II). The current density (J_e) value at an applied field of

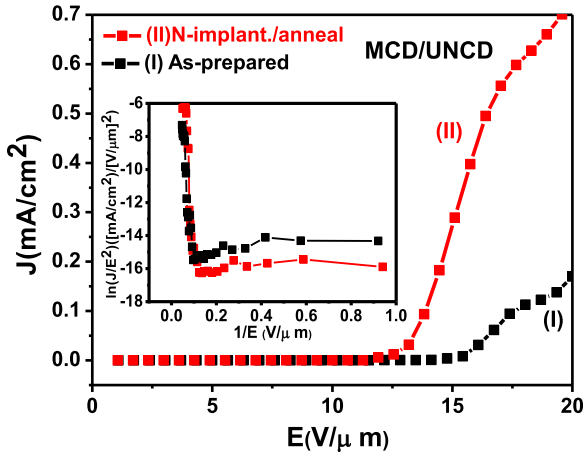

FIG. 1. Electron field emission properties of (I) as-prepared and (II) N-ion implanted/post-annealed hybrid-UNCD films. The inset shows the F–N plot of the corresponding J-E graph.

17 V/μm increases from 0.07 mA/cm^2 for as-prepared h-UNCD films to 0.57 mA/cm^2 for N-ion implanted/post-annealed films. The details of the EFE properties of as-prepared, N-ion implanted/post-annealed h-UNCD films are listed in Table I.

To understand the mechanism behind the enhancement in EFE properties for N-ion implanted/post-annealed films further, SEM, Raman, XPS, TEM, STM, and STS measurements are carried out in more detail. Figures 2(a) and 2(b) show the FESEM images of as-prepared and N-ion implanted/post-annealed h-UNCD films, respectively. Interestingly, the as-prepared h-UNCD (Fig. 2(a)) films do not show the surface morphology of either UNCD films grown in CH_4/Ar plasma or diamond films grown in hydrogen-containing plasma ($CH_4/Ar/H_2$). The surface of as-prepared h-UNCD films has few nanometres of diamond grains merged with each other, forming aggregates of about 100–200 nm in size. Interestingly, after the high dose ion implantation, deep groovings along the boundaries of the aggregates are observed (not shown). Post-annealing process seems to fuse together the groovings, making the surface look like true cauliflower structures (Fig. 2(b)).

Figures 3(a) and 3(b) show the Raman spectra of as-prepared and N-ion implanted/post-annealed h-UNCD films. The Raman spectra were de-convoluted by using multi-peak Lorentzian fitting method. Seven peaks were observed in as-prepared h-UNCD films as ν_1 (1133 cm^{-1}), ν_2 (1192 cm^{-1}), ν_3 (1450 cm^{-1}), D (1321 cm^{-1}), D* (1362 cm^{-1}), G (1552 cm^{-1}), and the nanographitic G′ (1594 cm^{-1}) as illustrated in Fig. 3(a). D-band resonance peak at 1321 cm^{-1} is the characteristic of diamond phase. The ν_1 and ν_2 refer to the signature of

TABLE I. The EFE performances of as-prepared and N-ion implanted/post-annealed hybrid-UNCD films (E_0, turn-on field estimated from the Fowler-Nordheim plots as the interception of the line segment extrapolated from high field and low field regime; J_e, EFE current density at an applied field of 17 V/μm).

Hybrid-UNCD samples	E_0 (V/μm)	J_e (mA/cm^2)
As-prepared	10.3	0.07
N-ion implanted/post-annealed	7.4	0.57

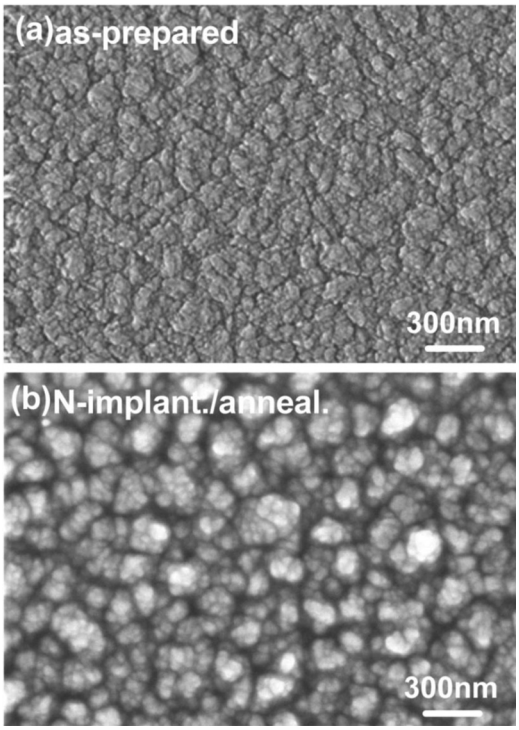

FIG. 2. SEM micrograph of (a) as-prepared and (b) N-ion implanted/post-annealed hybrid-UNCD films. Change in microstructure by the N implantation/post-annealing process is clearly seen.

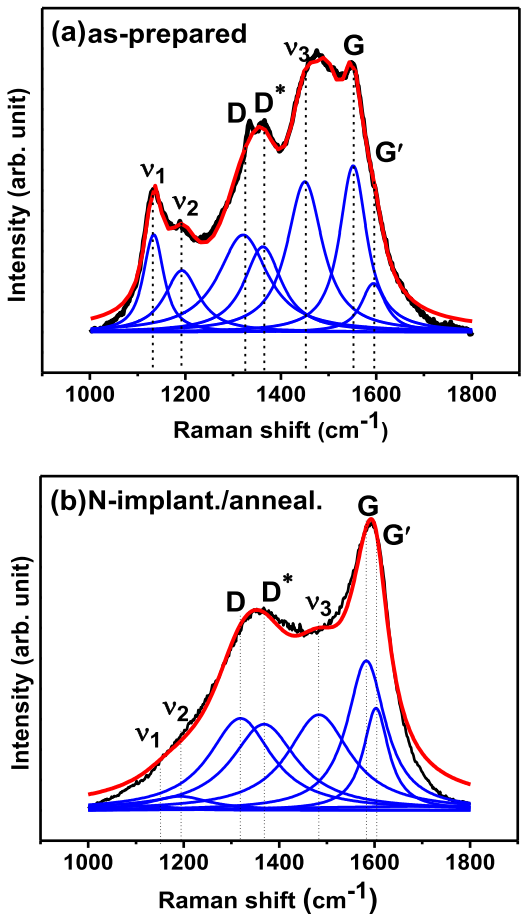

FIG. 3. Raman spectra of (a) as-prepared and (b) N-ion implanted/post-annealed hybrid-UNCD films taken with 514.5 nm laser line.

nanodiamond phase and always accompanied by another peak ν_3 due to the presence of transpolyacetylene (*trans*$(CH)_x$) phase at the grain boundaries.[14] Moreover, D*-band ($1362\,cm^{-1}$) and G-band ($1552\,cm^{-1}$) represent the disorder carbons and graphitic content in the diamond film, respectively.[15,16] A shoulder peak around $1594\,cm^{-1}$ (designated as G′ band) is seen that possibly arises from the nanocrystalline graphitic content of the films.[16]

The effect of N-ion implantation/post-annealing processes on altering the bonding characteristics of h-UNCD films is shown in Figure 3(b). Smaller amount of ν_1 and ν_2 phases is seen in N-ion implanted/post-annealed films. However, the position of ν_3 peak is shifted to higher wave number side ($1463\,cm^{-1}$). The shifting is probably a sign of the breaking of transpolyacetylene chains due to the high doses of N-ion implantation/post-annealing processes.[14] These processes increase markedly the D* peak, inferring the increase in disordered carbon and nano-graphitic phase. The Raman spectra show that I_G/I_D values (ratio of intensities of G-peak to D-peak) are 0.54 and 1.02 in as-prepared and N-ion implanted/post-annealed h-UNCD films, respectively. The increase of I_G/I_D value in N-ion implanted/post-annealed films indicates the formation of nanographite and decrease in sp^3 content, according to the three-stage model of increasing disorder in carbon materials.[16,17] It is to be noted that visible Raman spectroscopy can only give information about the sp^2-bonded carbon and only indirect information on the relative sp^3 content. The higher intensity of G′-band is observed after the N-ion implantation/post-annealing process (Fig. 3(b)). The disorder/amorphous type Raman resonances are converted into graphitic one due to the N-ion implantation/post-annealing of h-UNCD films. The position of G′ peak is 1594 and $1603\,cm^{-1}$ in as-prepared and N implanted/post-annealed films, respectively. The shifting of the G′ peak to higher wave number side in N-implanted/post-annealed films is possibly due to the formation of nanocrystalline graphite from amorphous phase by these processes.[16] The formation of nanographitic phase by the N implantation and post-annealing process is also confirmed by TEM study, which will be discussed shortly. The presence of defects, increase in sp^2 content upon N-implantation/post-annealing processes, and the presence of nanographitic phase can enhance the field emission properties of h-UNCD films.[13]

To reveal the effect of N ion implantation/post-annealing processes on the surface chemical bonding characteristics of h-UNCD films more precisely, XPS measurements were carried out. Figure 4 shows the C1s photoemission spectra of as-prepared and post-annealed h-UNCD films. The background was subtracted using Shirley's method.[18] The measurements were conducted without ion sputtering etching in XPS chamber to avoid reconfiguration of the surface bonding structures. The data were fitted with Lorentzian peaks with binding energies at 284.5, 285.6, 285.2, and 286.1 corresponding to the sp^2 (C=C), sp^3 (C–C), C=N, and C–N phases respectively. The relative intensities of each phase are given in Table II. In as-prepared h-UNCD, sp^3 C–C bonding is predominant with a peak intensity of 53.9% while sp^2 C=C intensity is 42.9%. There is a little amount of nitrogen present in as-prepared films as C–N (1.9%) and

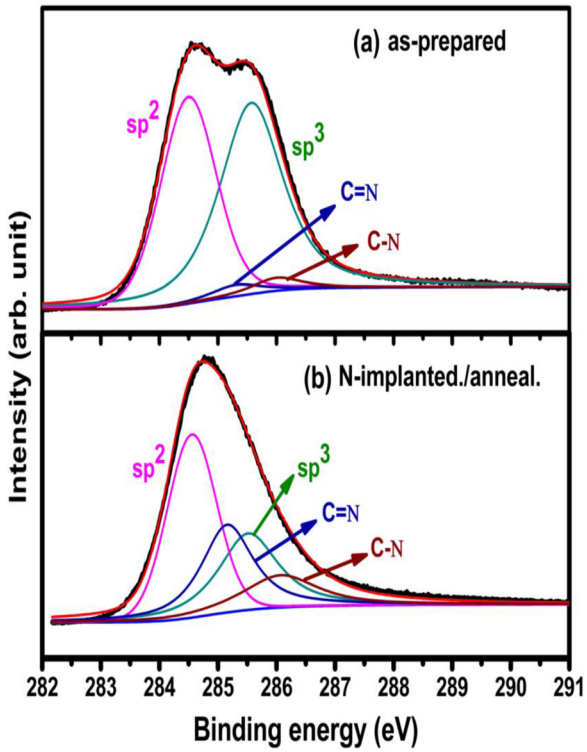

FIG. 4. C1s XPS spectra of (a) as-prepared and (b) N-ion implanted/post-annealed hybrid-UNCD films.

TABLE II. Relative intensities of various components of C1s XPS spectra from as-prepared and N-implanted/post-annealed hybride-UNCD films.

		Peak intensity (%) of hybrid-UNCD film	
Peak position (eV)	Chemical bonding	As prepared	Post-annealed
284.5	sp^2	42.9	46.8
285.6	sp^3	53.9	24.37
285.2	C=N	1.3	21.04
286.1	C–N	1.9	7.79

C=N (1.3%) phases. After **N-implantation**/post-annealing processes, sp^3 C–C peak intensity drastically decreases to 24.37% and sp^2 C=C peak intensity increases to 46.80%. Moreover, the **N-implanted**/post-annealed films clearly show the presence of C–N and C=N phases as marked in Fig. 4(b). The appearances of these phases indicate that the chemical bonding between C and N is formed after the **N-implantation**/post-annealing processes. The increase in sp^2 content upon **N-implantation**/post-annealing processes is consistent with the Raman results (Fig. 2(b)). Increase in C=N phase and decrease in C–N phase in **N-implanted**/post-annealed films indicate the loss of N atoms from the tetrahedral sp^3 site and increase in N atoms in aromatic sp^2 (C=C) sites. There will be also some loss of nitrogen and rearrangement of carbon atoms to form sp^2 C=C bonds.[19]

B. Scanning tunnelling spectroscopy

To reveal how the changes in microstructure and concentrations of sp^2, sp^3, C–N, and C=N phases affect the EFE properties of these films, the local electronic properties of the films were investigated by CITS in STS mode to directly reveal the emission sites in these films. STS measurements of as-prepared and N-implanted/post-annealed h-UNCD films were systematically performed to study the effect of these processes on the density of emission sites. As prepared h-UNCD films are resistive for STM measurements. The surface of as-prepared h-UNCD film became conducting when sputter ion-etched with Ar^+ ions for 1 min by removing nearly 1 nm thickness inside the XPS chamber. STM measurements are made after that Figure 5(a) shows the STM image of as-prepared h-UNCD film surface. In as-prepared h-UNCD films, the grains coalesced, forming bigger diamond aggregates, as also seen by SEM (cf. Fig 2(a)). Such a typical bigger diamond aggregate is marked as "*i*" with the facet as "*ii*" in Fig. 5(a). Figure 5(b) is the CITS image corresponding to Fig. 5(a) taken at a sample bias of −2.5 V. Bright and dark regions in the CITS image are visible with their shapes having similarity with the shapes of grain "*i*" and facet "*ii*" of STM image in Fig. 5(a), respectively. Bright contrast in the CITS image represents better electron emission.[13] The CITS image reveals that the emission sites are mainly along the facets of the as-deposited h-UNCD films, very less in density and are seen discontinuously throughout the sample surface.

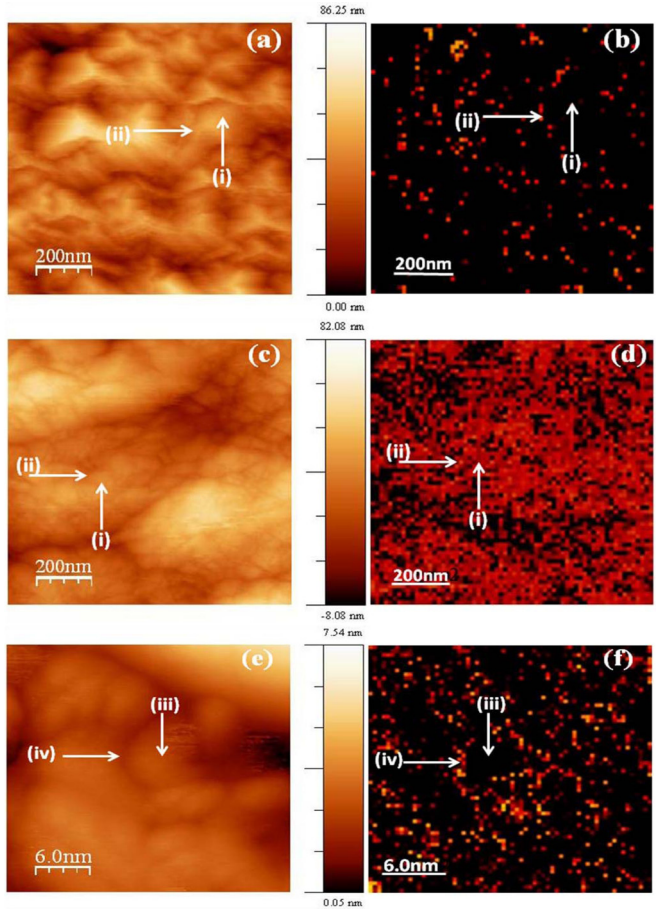

FIG. 5. The STM image of (a) as-prepared and (c) N-ion implanted/post-annealed hybrid-UNCD films with (b) and (d) showing the CITS image corresponding to (a) and (c); the HRSTM image of (e) N-ion implanted/post-annealed hybrid-UNCD films with (f) the corresponding CITS image. The CITS images were acquired at a negative sample bias of 2.5 V.

Figure 5(c) shows that coalesce of the smaller grains occurs due to the N-implantation/post-annealing processes and it forms typical cauliflower like structure as seen in SEM (cf. Fig. 2(b)). The corresponding CITS image is shown in Fig. 5(d), taken at a sample bias of −2.5 V. Typical large aggregates and boundaries in this image are marked as "*i*" and "*ii*." The corresponding positions in the CITS image (Fig. 5(d)) are also marked "*i*" and "*ii*." Interestingly, the emission site density increases significantly in N-implanted/post-annealed films than as-prepared films. It looks as if the whole film surface emits. The post-annealed h-UNCD film surface (Fig. 5(c)) is still made up smaller diamond particles. Figure 5(e) shows the high resolution STM (HRSTM) image taken within the diamond grain region marked as "*i*" in Fig. 5(c), which is actually composed of smaller grains separated by grain boundaries. We could observe uniform diamond grains of nearly 5 nm. Typical grain and grain boundary are marked as "*iii*" and "*iv*" in Fig. 5(e). Figure 5(f) shows the CITS image corresponding to Fig. 5(e) taken at the sample bias of −2.5 V. It is observed that the emission sites are along the grain boundaries of the smaller grains marked as "*iv*" in Fig. 5(f), indicating that grain boundaries are the prominent electron emission sites. Thus the larger grains observed in Fig. 5(c) are actually composed of smaller grains of nearly 5 nm in size, with well separated grain boundaries. The number densities of these smaller grains with emitting grain boundaries are large enough in N-implanted/post-annealed h-UNCD films such that it appears as if the bigger diamond aggregates as a whole emits when we see in a large scale.

The local electronic properties are characterized by measuring the local current vs. voltage (I-V) curves of N-ion implanted/post-annealed hybrid-UNCD films from STS measurements at various sample positions as on the grains and grain boundaries in HRSTM image shown in Fig. 5(e). The tunnelling current under positive bias to the h-UNCD films is lesser than that under negative bias, implying that the films have n-type conductivity. Only the negative portion of the I-V curves is shown in Fig. 6, as the negatively biased current corresponds to the tunnelling of electrons from the diamond surface to the tungsten tip and is proportional to the density of occupied states in the diamond. Ten reproducible I-V spectra corresponding to each emission sites (grain and grain boundaries of N-ion implanted/post-annealed film as shown in Fig. 5(e)) were recorded during the I-V measurements. It should be noted that the curves "G" and "GB" correspond to grain and grain boundary of N-ion implanted/post-annealed films, respectively (locations "*iii*" and "*iv*" in Fig. 5(e), respectively). We observed a significant change in I-V characteristic curves both at the grain and at the grain boundary for N ion implanted/post-annealed h-UNCD films. The grain boundaries (curve GB) emit at a lower sample bias compared to the grains (curve G). Moreover, the conductivity of the grain boundaries is better than that of grains in both films, which is consistent with the CITS image, showing bright emissions around the grain boundaries shown in Figs. 5(e) and 5(f).

Moreover, the I-V characteristic curves recorded during the STS measurements (Figure 6(a)) are used to calculate the normalized conductance $\frac{dI/dV}{I/V}$ at the grain and grain boundary

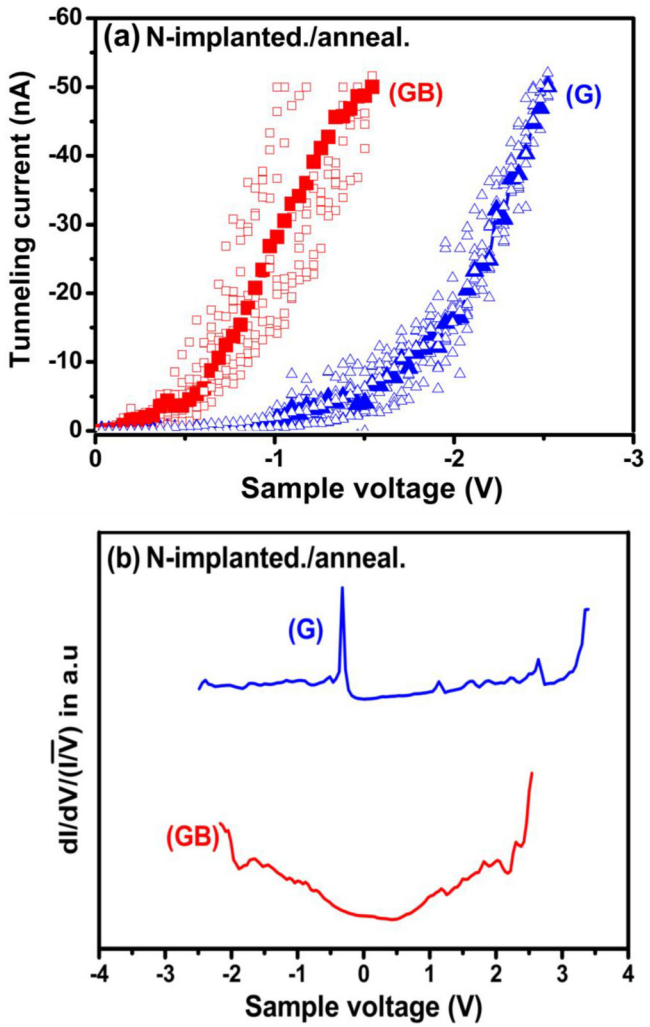

FIG. 6. The (a) local I-V curves obtained in STS measurements at the grain "G" and the grain boundary "GB" of N-ion implanted/post-annealed hybrid-UNCD films [marked as "*iii*" and "*iv*" in high resolution STM image in Fig. 5(e)], where the thick line drawn corresponds to the average of 10 I-V curves at the designated points. (b) Normalized differential conductance $(dI/dV)/(I/V)$ corresponding to I-V curves at the grain "G" and the grain boundary "GB" of these hybrid-UNCD films.

of the h-UNCD films. The normalized conductance vs. applied input voltage provides information about the surface local density of states (LDOS).[21,22] The normalized conductance curves corresponding to these I-V curves are plotted in Fig. 6(b) for N ion implanted/post-annealed films. From the I-V spectra corresponding to the grain of as-prepared h-UNCD films that were not shown here, we calculated a band gap of about 4.65 eV, which is in accorded with the reported value for the nanocrystalline diamond grain. Interestingly, the band gap decreases to 2.9 eV corresponding to curve "G" in Fig. 6(a) at the diamond grain in N-ion implanted/post-annealed hybrid-UNCD film as observed in curve "G," Fig. 6(b). The decrease in band gap is in accord with the band structure calculation[23] that showed the reduction in band gap of diamond by 25% after N doping. Furthermore, band gap of grain boundary reduces, showing nearly metallic behaviour (curve "GB," Fig. 6(b)). The sp^2, nanographitic phase, and nitrogen content at the grain boundaries increase by annealing process that gives rise to the observed metallic behaviour.

From the above described electronic band structure, we can assume that N ion implantation/post-annealing processes induce structural defects that can introduce electronic defect states in the band gap of diamond grains. This fact is also supported by the TEM results discussed shortly. Nitrogen substitution, which is confirmed by XPS measurements, can also introduce new electronic states in the band gap of diamond grains, as suggested by the density functional tight binding calculations of Zapol.[24,25] Moreover, band gap for the grain boundaries is much lesser, compared to that of the grains, due to the presence of a mixture of sp^2, sp^3, and amorphous carbon phases[26] (cf. TEM observations). The grain boundaries have higher conductivity that can account for the significant emission from these sites, as observed in the CITS images (cf. Fig. 5(f)).

Editing accepted N ion implantation/post-annealing processes remove the defects, form complex stable defects and conversion of amorphous phase to nano-graphite clusters, and enhance the doping of nitrogen and out diffusion of a certain fraction of nitrogen from diamond grains to the grain boundaries. Increase in DOS upon annealing can be due to the introduction of stable defect complexes in the diamond grain.[27] The high density of states within the band gap significantly reduces the potential barrier for field emitted electrons[28] and enhances the field emission properties.

Restated, densities of states are introduced in the band gap of diamond in N ion implanted/post-annealed films that enhances the EFE process. However, the grain boundaries mostly contain the nanographitic phase giving raise to metallic conductivity. These conductive grain boundaries form conducting channels at the interface of diamond grains, resulting in prominent electron emission. The grain boundaries are more susceptible to amorphization and graphitization upon the N implantation/post-annealing processes.[11] This is the authentic factor altering the EFE behaviour for these films. Our results show the possibility of a grain-boundary electron transport mechanism (conductivity-channel process)[24,28] in h-UNCD films.

C. Transmission electron microscopy

The STS measurements illustrate clearly the benefit of N ion implantation/post-implantation-annealing process on increasing the number density of field emission sites. However, the authentic factor for such an effect is still not clear. It is suspected that the modification on the granular structure for these films due to N ion implantation/post-annealing process is the key. To investigate the possible cause for such phenomena, the detail microstructure of these films was examined using TEM. Figures 7(a) and 7(b) show the bright field TEM micrographs of as-prepared and N-ion implanted/post-annealed h-UNCD films, respectively. Figure 7(a) reveals the microstructure of as-prepared h-UNCD films, viz., all the films contain large diamond aggregates dispersed evenly among the ultra-small grain matrix, forming a duplex-granular structure. The selected area electron diffraction (SAED) shown as inset in each figure contains ring shaped diffraction patterns, corresponding to (111), (220), and (311) lattices of diamond, which indicates that most of the materials are of diamond structure, even though Raman spectra show small or invisible resonance peaks corresponding to sp^3-bonds for the films. The diffraction spots are spotty and are arranged in a ring geometry, which infers the presence of large and randomly oriented diamond grains. N-ion implantation/post-annealing processes seem to impose very limit modification on the granular structure for these films, except that the large grains changed from equi-axed geometry to elongated rod geometry for the N-ion implanted/post-annealed samples (Fig. 7(b)). The duplex-granular structure is still preserved. Figure 7(c) shows the typical TEM micrograph for the ultra-small grain region in as-prepared and N-ion implanted/post-annealed hybrid-UNCD films, indicating that this region contains abundant nano-sized diamond grains (~5 nm) with very uniform size

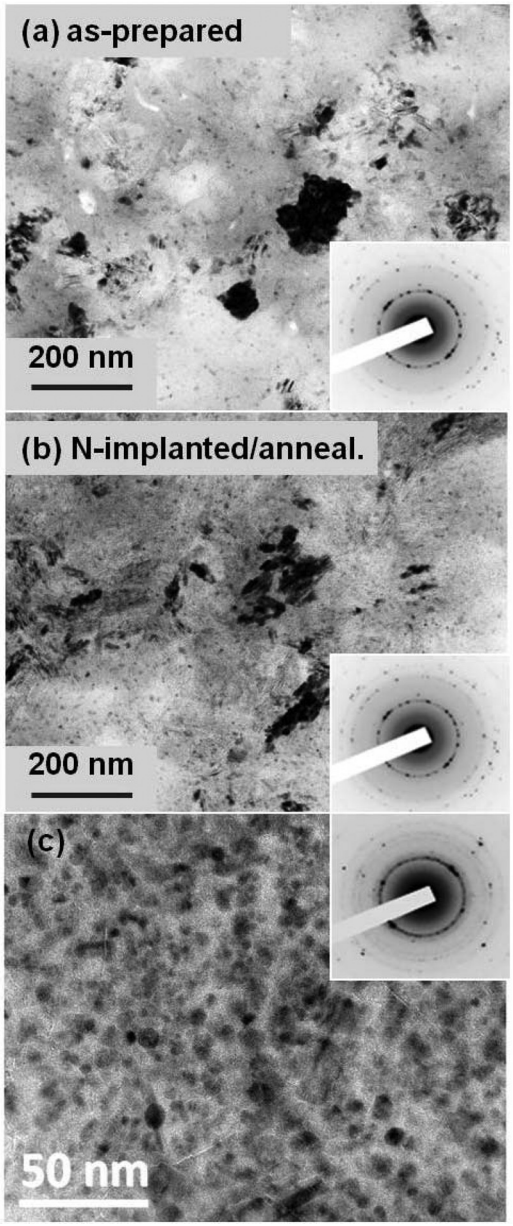

FIG. 7. The bright field TEM micrographs of (a) as-prepared and (b) N-ion implanted/post-annealed hybrid-UNCD films; (c) the bright field TEM micrograph of a typical ultra-small grain region in as-prepared or N-ion implanted/post-annealed hybrid-UNCD films.

distribution. It shows stronger central diffuse diffraction ring, indicating that the ultra-small grain regions contain much larger proportion of nano-graphite (or amorphous-carbon).

However, more detailed investigation using high resolution TEM revealed marked change in microstructure of the films induced by the N-ion implantation/post-annealing processes. Figure 8(a) shows the TEM structure images corresponding to the large diamond aggregates of the as-prepared h-UNCD films along with the associated Fourier-transformed (FT) diffractograms, which corresponding to whole structure image shown as insets (labelled as FT_{0a}). It shows that, in as-prepared h-UNCD films, the diamond aggregates contain large proportion of planar defects. There are regions containing parallel fringes with irregular spacing, region 1. The rel-rods associated with the major diffraction spots in the associated FT_1 image (inset, Fig. 8(a)) indicate that these fringes correspond to stacking faults.[20] There are regions containing parallel fringes with regular spacing, region 2. The systematic diffraction spots in FT_2 image (insets, Fig. 8(a)) implies that these fringes correspond to hexagonal diamond lattice,[20] an allotropy of cubic diamond. Figure 8(b) shows that the planar defects, including the stacking faults and hexagonal diamond lattices, are still observable but are less in proportion for the N-ion implanted/post-annealed hybrid-UNCD films. Moreover, there are regions where some irregularities were induced (indicated by arrows). These irregularities could be point defects (voids) or line defects (dislocations), as seen by the shifting in diffraction spots in the FT image (FT_4) corresponding to region 4, with respect to the regular diamond lattices (region 3 and FT_3) in Fig. 8(b). N-ions implantation/postannealing of h-UNCD films leads to recrystallization process, which converted the amorphous carbon into nanographites and induced the coalescences of the diamond grains.

Figures 9(a) and 9(b) show the TEM structure image for the ultra-small grain region of the as-prepared and N-ions implanted/post-annealed h-UNCD films, respectively. This indicates that there is large proportion of amorphous phase existing at the diamond grain boundaries that is implied by the FT images corresponding to the whole structure image (FT_{0a} and FT_{0b}). Notably, the diamond grains are smaller in size for N-ions implanted/post-annealed h-UNCD films, as compared with those of as-prepared ones, that are highlighted by FT_1, FT_3, and FT_4-images corresponding to regions 1, 3, and 4, respectively, in Figs. 9(a) and 9(b). The N-ions implantation/post-annealing processes seem to disintegrate the grain boundary transpoly-acetylene phase, induces the formation of nanographite at the grain boundary regions. Such an argument is supported by the presence of stronger central ring in the FT image, FT_{0b}.

Restated, the N-ion implantation/post-annealing processes markedly modify the microstructure of both the large diamond aggregates and the ultra-small diamond grains of the h-UNCD films. Substitutional incorporation of N ions into diamond occurs which is expected to alter the electronic band structure for diamond and can account for the change in band gap

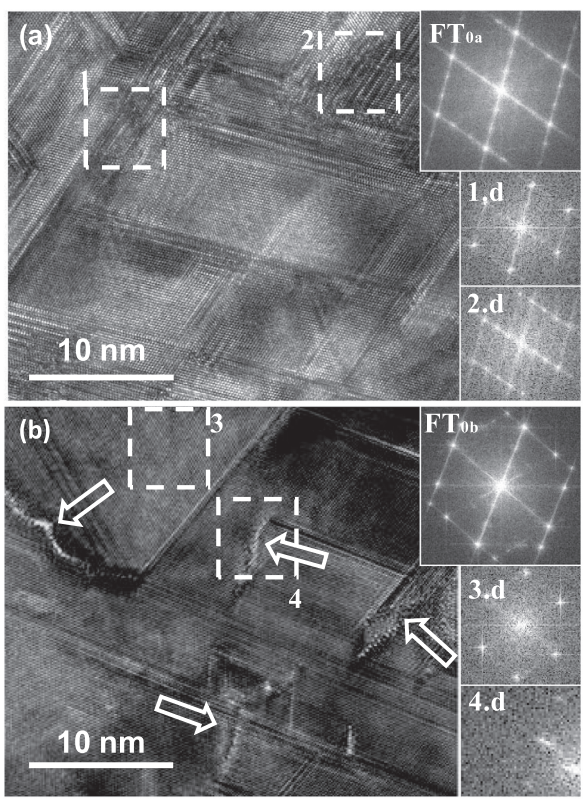

FIG. 8. The TEM structure image corresponding to the large diamond aggregates for (a) as-prepared and (b) N ion implanted/post-annealed hybrid-UNCD films. The insets FT_{0a} and FT_{0b} show the FT images corresponding to the whole structure images in "a" and "b," respectively, and the FT_1 to FT_4 show the FT images corresponding to the areas "1" to "4," respectively.

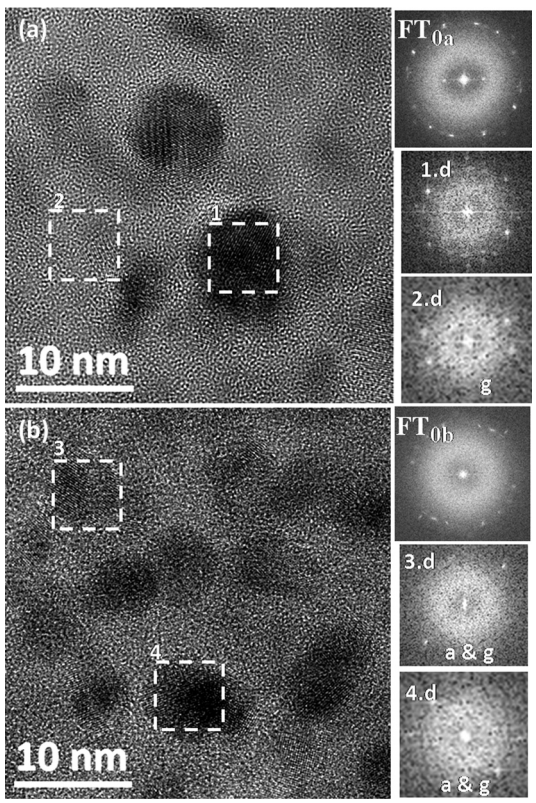

FIG. 9. The TEM structure image of a typical ultra-small grain region for the (a) as-prepared and (b) N-ion implanted/post-annealed hybrid-UNCD films. The insets FT_{0a} and FT_{0b} show the FT images corresponding to the whole structure images in "a" and "b," respectively, and the FT_1 to FT_4 show the FT images corresponding to the areas "1" to "4," respectively.

measurements. The modification on the electronic structure of the large diamond aggregates could facilitate the field emission behaviour for these films. However, more prominent effect due to these processes is the induction of nano-graphite phase between the ultra-small diamond grain regions that form an interconnected path for electron transport.

IV. CONCLUSION

The electron field emission properties of the two-step MPECVD grown diamond (hybrid-UNCD) films were markedly improved by N-ion implantation/post-annealing processes. N ion implanted/post-annealed hybrid-UNCD hybrid films show a low turn-on field of $((E_0)_{\text{hybrid-UNCD}} = 7.4\ \text{V}/\mu\text{m})$ with large current density of $((J_e)_{\text{hybrid-UNCD}} = 0.57\ \text{mA/cm}^2$, at $17\ \text{V}/\mu\text{m}))$, which is markedly better than the one-step prepared UNCD films. XPS measurements show increased sp^2 phase content and C–N bonding fraction in N ion implanted/post-annealed films. Microstructural analysis reveals the mechanism behind the enhanced EFE properties in N implanted/post-annealed films is due to the induction of point defects in the diamond grains and formation of nanographitic phase surrounding the small diamond grains. Current imaging tunnelling spectroscopy in scanning tunnelling spectroscopy mode directly shows the increased emission site densities in N implanted/post-annealed hybrid-UNCD films than the as-prepared ones. The role of nanographitic phase confirmed from TEM studies in improving the emission sites in N implanted/post-annealed films is directly revealed by high resolution CITS measurements. The nanographites surrounding the small diamond grain region formed an interconnected path throughout the film surface that facilitates the easy transport of electrons and thereby markedly enhances the EFE properties of these N implanted/post-annealed hybrid-UNCD films.

ACKNOWLEDGMENTS

The authors would like to thank Mr. Nandagopala Krishna for XPS and Mr. P. Shyamala Rao for FESEM experiments.

[1]T. D. Corrigan, D. M. Gruen, A. R. Krauss, P. Zapol, and R. P. H. Chang, Diamond Relat. Mater. **11**, 43 (2002).
[2]W. Zhu, G. P. Kochanski, and S. Jin, Science **282**, 1471 (1998).
[3]C. S. Wang, H. C. Chen, H. F. Cheng, and I. N. Lin, J. Appl. Phys. **105**, 124311 (2009).
[4]H. F. Cheng, C. C. Horng, H. Y. Chiang, H. C. Chen, and I. N. Lin, J. Phys. Chem. C **115**, 13894 (2011).
[5]H. F. Cheng, H. Y. Chiang, C. C. Horng, H. C. Chen, C. S. Wang, and I. N. Lin, J. Appl. Phys. **109**, 033711 (2011).
[6]S. Fan, M. G. Chapline, N. R. Franklin, T. W. Tombler, A. M. Cassell, and H. Dai, Science **283**, 512 (1999).
[7]S. Pandey, P. Rai, S. Patole, F. Gunes, G. D. Kwon, J. B. Yoo, P. Nikolaev, and S. Arepalli, Appl. Phys. Lett. **100**, 043104 (2012).
[8]M. Qian, T. Feng, H. Ding, L. Lin, H. Li, Y. Chen, and Z. Sun, Nanotechnology **20**, 425702 (2009).
[9]J. F. Prins, Diamond Relat. Mater. **10**, 1756 (2001).
[10]R. Kalish, Carbon **37**, 781 (1999).
[11]C. Uzan-Saguy, C. Cytermann, R. Brener, V. Richter, M. Shaanan, and R. Kalish, Appl. Phys. Lett. **67**, 1995 (1194).
[12]K. Panda, B. Sundaravel, B. K. Panigrahi, P.-C. Huang, W.-C. Shih, H.-C. Chen, and I.-N. Lin, J. Appl. Phys. **111**, 124309 (2012).
[13]R. H. Fowler and L. Nordheim, Proc. R. Soc. A **119**, 173 (1928).
[14]A. C. Ferrari and J. Robertson, Phys. Rev. B **63**, 121405 (2001).
[15]J. Michler, Y. Von Kaenel, J. Stiegler, and E. Blank, J. Appl. Phys. **83**, 187 (1998).
[16]A. C. Ferrari and J. Robertson, Phys. Rev. B **61**, 14095 (2000).
[17]A. Ilie, A. C. Ferrari, T. Yagi, S. E. Rodil, J. Robertson, E. Barborini, and P. Milani, J. Appl. Phys. **90**, 2024 (2001).
[18]Y. F. Chen, Surf. Sci. **380**, 199 (1997).
[19]J. J. Li, W. T. Zheng, H. H. Wu, L. Sun, G. G. Gu, H. J. Bian, X. Y. Lu, and Z. S. Jin, J. Phys. D: Appl. Phys. **36**, 2001 (2003).
[20]I. N. Lin, H. C. Chen, C. S. Wang, Y. R. Lee, and C. Y. Lee, Cryst. Eng. Comm. **13**, 6082 (2011).
[21]R. M. Feenstra, Surf. Sci. **965**, 299 (1994).
[22]R. M. Feenstra and P. Martenssion, Phys. Rev. Lett. **61**, 447 (1988).
[23]J. W. Park, C. W. Sohn, and B. H. Choi, Curr. Appl. Phys. **6**, 188 (2006).
[24]P. Zapol, M. Sternberg, L. A. Curtiss, T. Frauenheim, and D. M. Gruen, Phys. Rev. B **65**, 45403 (2001).
[25]V. I. Polyakov, A. I. Rukovishnikov, N. M. Rossukanyi, V. G. Pereverzev, S. M. Pimenov, J. A. Carlisle, D. M. Gruen, and E. N. Loubnin, Diamond Relat. Mater. **12**, 1776 (2003).
[26]E. Rohrer, C. F. O. Graeff, R. Janssen, C. E. Nebel, H. Guettler, and R. Zachai, Phys. Rev. B **54**, 7874 (1996).
[27]O. A. Williams, M. Nesladek, M. Daenen, S. Michaelson, A. Hoffman, E. Osawa, K. Haenen, and R. B. Jackman, Diamond Relat. Mater. **17**, 1080 (2008).
[28]O. A. Williams, S. Curat, J. E. Gerbi, D. M. Gruen, and R. B. Jackman, Appl. Phys. Lett. **85**, 1680 (2004).